Vortex Street Dynamics: The Selection Mechanism for the Areas and Locations of Jupiter's Vortices

TOM HUMPHREYS

Atmospheric Sciences Division, Lawrence Livermore National Laboratory, Livermore, California

PHILIP S. MARCUS

Department of Mechanical Engineering, University of California, Berkeley, Berkeley, California

(Manuscript received 11 March 2005, in final form 21 July 2006)

ABSTRACT

With the exception of the Great Red Spot, Jupiter's long-lived vortices are not isolated, but occur in east–west rows. Each row is centered about a westward-going jet stream with anticyclones on the poleward side and cyclones on the equatorial. Vortices are staggered so that like-signed vortices are never longitudinally adjacent. These double rows of vortices, called here Jovian vortex streets (JVSs) are robust. Calculations with no forcing and no dissipation (i.e., Hamiltonian dynamics) allow a continuum of JVS solutions, so they cannot be used to determine the physics that selects the observed values of the areas, circulations, and locations of Jupiter's vortices. Constraints imposed by stability put few bounds on these values. When small amounts of dissipation and forcing are added to the governing equations, there is no longer a continuum of solutions; an initial JVS that was a solution of the Hamiltonian equations is now out of equilibrium and evolves to an attractor. For fixed forcing, all initial JVS evolve to the same attractor, so that the area of the vortices in the late-time JVS is selected uniquely as is the separation width in latitude between the row of cyclones and row of anticyclones. The separation width of the attracting JVS is nearly independent of the forcing, but the areas of the vortices in the attracting JVS depend strongly on the strength of the forcing, which is a measure of the ambient Jovian turbulence. Results are compared with observations.

1. Introduction and motivation

The Jovian weather layer (containing the visible clouds) is characterized by vortices and a zonal system of jet streams (Fig. 1). Assuming the jet streams are indicated by Jupiter's multicolored bands, they have persisted for at least 340 years (Hook 1665). Their averaged east–west velocity $\overline{\mathbf{v}}(y)$ as a function of latitude y was nearly unchanged from 1979 (Limaye 1986), through the early 1990s (Simon and Beebe 1996) to 2006 (P. S. Marcus et al. 2006, unpublished manuscript). Vortices appear at almost all latitudes more than 15° from the equator. However, with the exception of the Great Red Spot (GRS), they are not isolated, but rather occur in east–west rows that straddle one of the westward-going jet streams with anticyclones (cyclones) on the poleward (equatorial) side of the jet stream (Fig. 1). Cyclones are interspersed in longitude between anticyclones, so that like-signed vortices are never longitudinally adjacent (Marcus 2004). In this configuration, which we call a Jovian vortex street (JVS), the centers of the anticyclones (cyclones) are embedded in an average zonal shear $\overline{\sigma}(y) \equiv -d\overline{\mathbf{v}}/dy$ that is also anticyclonic (cyclonic). This is in accord with theory (Marcus 1988, 1990; Dritschel 1990) and experiment (Sommeria et al. 1989): vortices thrive when the sign of the vortex and ambient shear are the same, but torn apart otherwise. Although cyclones and anticyclones in a JVS can be centered at nearly the same latitude (cf. the vortices near 40°S in Fig. 2), the westward jet stream is displaced so that it meanders between them (Fig. 3b), keeping cyclones on one side and anticyclones on the other.

We argued previously that without forcing and dissipation there is a continuum of stable JVSs (Marcus 1993). Mathematically, the vortices in a JVS can have

Corresponding author address: Philip S. Marcus, 6121 Etcheverry Hall, University of California, Berkeley, Berkeley, CA 94720. E-mail: pmarcus@me.berkeley.edu

DOI: 10.1175/JAS3882.1

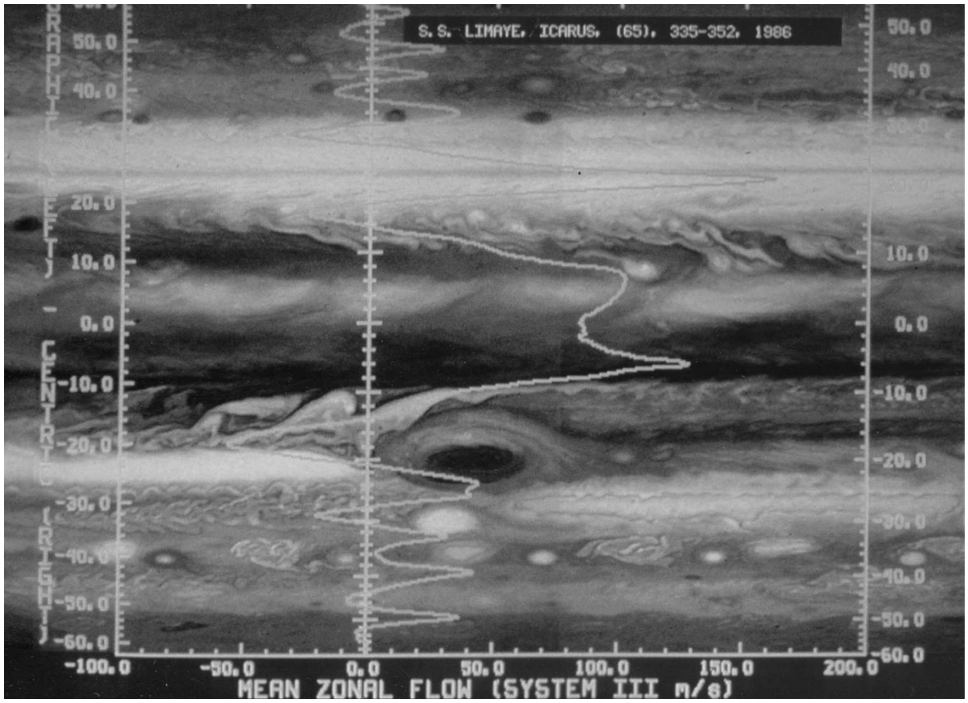

FIG. 1. *Voyager* mosaic (Limaye 1986). The superposed white line is the averaged zonal velocity $\bar{\mathbf{v}}(y)$. Rows of cyclones and anticyclones straddle each of the westward-going jet streams with the cyclones (anticyclones) on the equatorial (poleward) sides. The clouds of the anticyclones are elliptical, compact, and bright, whereas those of the cyclones are tangled, wispy filaments.

wide ranges of areas, potential vorticities and locations in latitude. Some additional physics must therefore select the observed Jovian values, and this paper explores them. If vortices do not merge and if there were no dissipation and no forcing, those quantities remain fixed at their initial values. Considering the extreme ages of the Jovian vortices and the forcing and dissipation in the Jovian atmosphere, it does not seem plau-

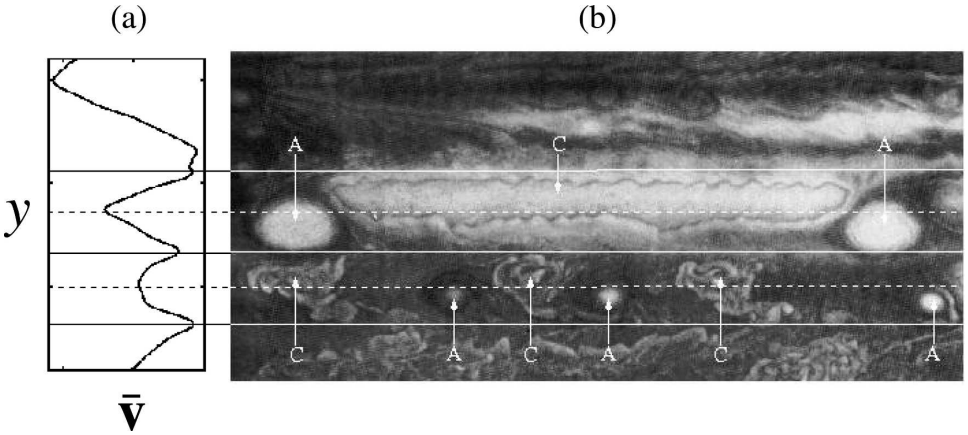

FIG. 2. (a) Velocity of the azimuthally averaged zonal flow $\bar{\mathbf{v}}$ as a function of latitude λ (from Fig. 1), with the locations of the maximum eastward-going jet streams shown as solid lines at $\lambda = 28°$, 36° and 44°S and the maximum westward-going jet streams as broken lines at $\lambda = 33°$ and 40°S. (Latitudes in this article are planetographic.) (b) A *Voyager* mosaic showing one anticyclone and two cyclones straddling the jet stream at 33°S and three anticyclone/cyclone pairs straddling the jet at 40°S. The centers of the cyclones (anticyclones) are shown with a C (A). The vortices are so large that the cyclones and anticyclones in the same JVS overlap in latitude.

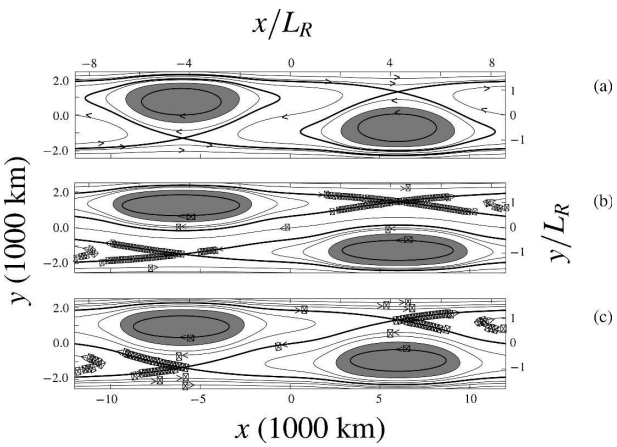

FIG. 3. Numerical calculation of JVSs. JVSs are classified as type I, II, or III, in accord with the number of stagnation points on the OCS around each vortex (see section 4 for details and parameter values). Vortices are shaded and all have $A = 1.1 \times 10^7$ km^2. Because the JVSs in the reference frame of this figure are steady, the vortex boundaries are also streamlines. Each OCS (thick curve) is a separatrix that divides the fluid into a region where fluid circulates around the planet and regions where the fluid is trapped on closed streamlines in or near a vortex. OCSs cross at stagnation points. (a) Type I ($W = 1400$ km). Type I and III JVSs appear to have no westward-going jet stream, but an azimuthal-average (as in Fig. 1) of the east–west velocity shows a westward-going jet stream. (b) Type II ($W = 2600$ km). The westward-going jet streamlines meander between large vortices. (c) Type III ($W \simeq 1860$ km). The unique westward-going jet streamline is punctuated with stagnation points.

sible that their current properties reflect initial conditions. In fact, large changes in areas and latitudes of the three White Oval anticyclones (that made up half of the JVS at 33°S) are well documented from their birth in 1939–41 (Rogers 1995) to their demise, beginning in 1998. We consider Jovian vortex streets, rather than individual vortices, to be the fundamental coherent features of the Jovian atmosphere. Other than our own nearly dissipation-less studies of JVSs (Marcus 1993; Youssef and Marcus 2003; Marcus 2004), we know of no other studies of their dynamics. The goal of this paper is to determine whether a simplified, but physically motivated, model of forcing and dissipation drives the JVS, regardless of initial conditions, to a unique, late-time solution and thereby determines its late-time properties. We are interested in isolating the mechanisms that evolve a JVS toward its attractor. Since this is the first study of the long-term behavior of a JVS, and since there is much uncertainty in determining the areas, potential vorticities and, in some cases, even the number of vortices in Jupiter's vortex streets, our strategy is to be as general as possible rather than to try to model precise Jovian conditions. For example, within each vortex street the absolute values of the potential vorticities of Jupiter's cyclones and anticyclones differ, but here for simplicity, we usually make them equal. Therefore, we shall generally make only qualitative comparisons between our results and Jovian observations.

In section 2 we review the differences among the dynamics of a few isolated patches of vorticity, of a vortex embedded in a shear flow, and of vortices in a JVS. Most studies of vortex dynamics (Dritschel 1986; Pullin 1998; Saffman 1992; Chorin 1997) were carried out with isolated patches of vorticity, and the intuition based on those dynamics is often misleading when applied to a JVS. In section 3, we review the governing equations. In section 4, we compute steady and time-dependent JVSs with no forcing or dissipation. All initial-value calculations of Jovian vortices with no forcing and no dissipation (Ingersoll and Cuong 1981; Dowling and Ingersoll 1988; Marcus 1988; Cho and Polvani 1996; Williams and Yamagata 1984), have "rigged" initial conditions, chosen so that the values of the conserved quantities, such as circulation and energy, of the initial conditions match those of the desired late-time vortices. Therefore, in section 5, we introduce forcing and dissipation and show that vortices evolve to attractors with unique values of area and locations in latitude. The section begins by demonstrating that standard numerical methods cannot be used for evolving a JVS with forcing and dissipation for the required ~5000 vortex turn-around times. A model using a numerical method that can be evolved that long is introduced. In section 6 we carry out numerical experiments to explain the physics of our results. Our conclusions and their relations to Jovian observations are in section 7.

2. Review of Jovian vortex streets—Theory and observations

a. Vortices embedded in a shearing zonal flow

Jovian vortices are embedded in a zonal shearing flow $\overline{\mathbf{v}}(y)$, and its shear $\overline{\sigma}(y)$ significantly modifies vortex behavior (Marcus 1988, 1990; Dritschel 1990). One modification is that an unembedded vortex with sharp boundaries (especially when approximated as a piecewise constant patch of vorticity and computed with contour dynamics) continually sheds thin filaments of vorticity (Dritschel 1988), while an embedded vortex only creates filaments when it encounters stagnation points. Another is that the shape of an unembedded vortex, and therefore its self-energy, is strongly affected by nearby vortices [cf. V states (Deem and Zabusky 1978)]. In contrast, the shape, and in particular the aspect ratio, of an embedded vortex is largely determined by the ratio of its ambient shear $\overline{\sigma}(y)$ to its own poten-

tial vorticity [cf. the family of vortices found by Moore and Saffman (1971)]. As embedded vortices evolve, their shapes are nearly rigid and elliptical except when they have close encounters with each other or with stagnation points. The boundaries of embedded vortices are usually sharp, characterized by steep gradients of the potential vorticity. Numerical simulations and experiments (Sommeria et al. 1989) show that the shearing zonal flow exterior to a collection of interacting vortices mixes and homogenizes the exterior zonal potential vorticity; similarly, the potential vorticity within each vortex homogenizes, so that the overall flow can be approximated as having piecewise-constant potential vorticity. This same piecewise-constant approximation has also been noted for Jupiter's zonal velocity (Read et al. 2006) and has been used for modeling it and other planetary zonal flows and vortices (Polvani et al. 1990; Cho et al. 2001). The best-observed JVS was at 33°S, containing the three White Ovals. Youssef and Marcus (2003) studied the mergers of the White Ovals and found good agreement with the observations, including the vortex shapes, by modeling the anticyclones as nearly uniform patches of potential vorticity of magnitude $1.1 \times 10^{-4}\ \mathrm{s}^{-1}$, each with area $4.5 \times 10^{7}\ \mathrm{km}^2$ and cyclones with potential vorticity $-4.7 \times 10^{-5}\ \mathrm{s}^{-1}$. Treating the anticyclones in the JVS at 40°S as patches of uniform potential vorticity of strength $6 \times 10^{-5}\ \mathrm{s}^{-1}$ reproduces their shapes well.

b. Small north–south displacements create large east–west velocities

Jovian vortices advect with the ambient velocity (see section 3). They drift primarily east and west, rather than north or south, because $\overline{\mathbf{v}}(y)$ dominates the weather layer. [In the special case that $\overline{\mathbf{v}}(y)$ has uniform potential vorticity, the drift speed of an isolated vortex is equal to $\overline{\mathbf{v}}(y_0)$, where y_0 is the latitude of the center of potential vorticity of the vortex (Marcus 1993).] However when the separation between vortices becomes less than approximately the Rossby deformation radius L_R (defined in section 3), the circumferential velocity around each vortex influences its neighbors as much as $\overline{\mathbf{v}}$. Neighboring vortices then move north or south, changing their latitude by δy. [At distances greater than L_R, the velocity created from an isolated patch of potential vorticity falls exponentially fast (Marcus 1993).] Although δy is small, the large shear $\overline{\sigma}(y)$ creates a large change in a vortex's east–west drift velocity:

$$\delta\overline{\mathbf{v}} \simeq -\overline{\sigma}\delta y. \tag{1}$$

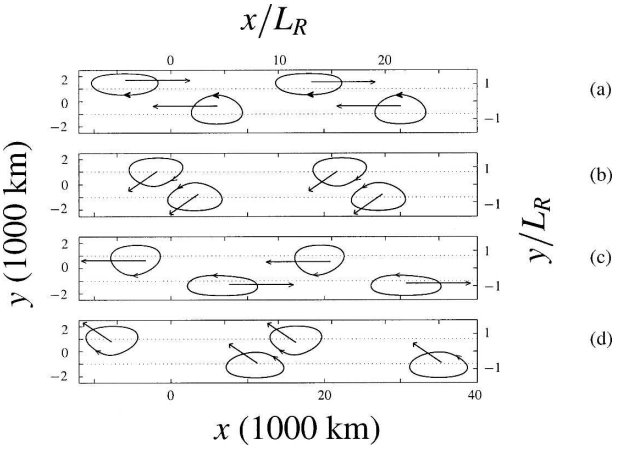

FIG. 4. Calculation of a time-dependent, oscillating JVS at 4 times during the elongated orbit of a vortex. Parameter values are as in section 4 with $W = 2000$ km and $A = 1.1 \times 10^7$ km^2 (a type II JVS). Straight arrows indicate the mean motion of the vortices at those times and show why opposite-signed vortices repel. If the amplitudes of the oscillations were infinitesimal this would be the primary eigenmode, and the flow would be periodic in time. Vortices orbit around the locations of the vortex centers of the steady-state or reference JVS (defined in section 4b), and the dotted lines indicate the latitudes of those centers. The distance between the dotted lines is the width W of the reference JVS. To a first approximation, the zonal flow between the dotted lines is to the west, and outside the lines to the east. Therefore when a vortex lies between the dotted lines, it advects to the west; when outside the lines, to the east. In the upper (lower) half of each subfigure the shear $\overline{\sigma}(y)$ is negative (positive).

c. Repulsion between opposite-signed vortices in a JVS

Inevitably, vortices near the same latitude that are embedded in a zonal shear $\overline{\sigma} \neq 0$ approach each other due to the differential east–west velocities. In numerical simulations, regardless of whether they are two-dimensional (Marcus 1988; Dowling and Ingersoll 1988, 1989; Marcus 1990) or three-dimensional (Morales-Juberias et al. 2003; Barranco and Marcus 2005), when like-signed, vortices at about the same latitude come within a few L_R, they merge on an advective time scale. In contrast, opposite-signed, embedded vortices at approximately the same latitude that straddle a westward jet stream repel (Marcus 1993; Youssef and Marcus 2003; Marcus 2004); it is this repulsion that makes a JVS stable. To understand the repulsion, consider a clockwise-rotating vortex approaching the western side of a counterclockwise vortex as in Fig. 4a. The circumferential rotation around the vortices displaces both southward, so both have displacements $\delta y < 0$ as in Fig. 4b. Because the westward jet passes between the two opposite-signed vortices, the ambient shear of the counterclockwise (clockwise) vortex is positive (negative).

With Eq. (1), the change in east–west drift velocity $\delta\bar{\mathbf{v}}$ of the counterclockwise (clockwise) vortex is positive (negative) and toward the east (west) as in Fig. 4c. The repulsion is similar when a clockwise vortex approaches the eastern side of a counterclockwise vortex as in Fig. 4d. The repulsion in Fig. 4 was seen in many *Voyager* observations in which anticyclones reverse directions. MacLow and Ingersoll (1986) describe one observation as follows: "Event III involves an anticyclonic spot [clockwise vortex in Fig. 4a] in the northern hemisphere that approaches from the west and encounters a cyclonic FR (filamentary region) [counter-clockwise vortex in Fig. 4a], which is at slightly lower latitude than the spot. The spot moves equatorward [south], passing to the west of the cyclonic region [as in Fig. 4b] before retreating back to the west at a lower latitude [as in Fig. 4c]."

d. Eigenmodes and time-dependent, oscillating JVS

A vortex street made of N point vortices with infinite deformation radius L_R that is not embedded in a zonal flow $\bar{\mathbf{v}}$ is unstable for all but a single value of the ratio of its vortex spacings (i.e., separation in streetwise direction x to separation in street-width direction y; Lamb 1945). With finite L_R, there is a small range of spacings where JVSs are not unstable (Masuda and Miki 1995). In contrast, all $N/2$ of a JVS eigenmodes are neutrally stable (i.e., are neither growing nor decaying) and temporally periodic when the JVS is made of point vortices embedded in a zonal flow with a westward-going jet between the two rows (see section 3 for details), regardless of the spacing (except when the zonal shear $\bar{\sigma}$ is very weak). The eigenmodes consist of the point vortices orbiting about their steady-state equilibrium locations. The eigenmodes of a JVS with finite-area vortices are similar to those with point vortices and are also similar to the finite-amplitude orbits shown in Fig. 4. The orbits that the vortices follow are highly elongated in the streetwise, or east–west, direction even for small amplitudes, so in most cases the vortices appear only to oscillate in longitude. Even a weakly nonlinear orbit has an east–west diameter that is close to the maximum value of $\sim 2\pi R_J/N$ ($\sim$50 000 km for the White Ovals), where $2\pi R_J$ is the local latitudinal circumference of the planet and N is the number of vortices in the JVS. In contrast, the north–south orbital diameter $2\Delta y$ is much smaller [$\sim$1000 km for the White Ovals (Rogers 1995)].

e. Definition of vortex and uncertainties in Jovian observations

The definition of a Jovian vortex is ambiguous in the literature. Since the Jovian vortices are embedded in a background zonal flow that has shear and vorticity almost everywhere, we define a vortex as a compact region of potential vorticity that is very different or anomalous to the background potential vorticity of $\bar{\mathbf{v}}$. As a counter example to our definition, the Southern Equatorial Belt (SEB) is a cyclonic region of closed streamlines just north of the GRS that might be considered a long-lived vortex. However, consider the thought experiment of a fluid consisting of a set of alternating zonal flows that is periodic in the east–west direction (cf. the Jovian jet streams) and place an anticyclone (cf. the GRS) in one of the anticyclonic bands. The north–south velocity of the anticyclone alters the streamlines of the surrounding cyclonic belts. In particular, the formerly parallel streamlines in the cyclonic region north of the anticyclone change to closed streamlines (cf. the SEB). However those streamlines, by construction, are not those of an anomalous patch of potential vorticity. For these reasons we do not consider the SEB to be a vortex. To prove directly that the SEB is not an anomalous vorticity patch is difficult because it requires the differentiation of noisy velocity measurements. However if the SEB did have an anomalous potential vorticity, then it and the GRS would oscillate back-and-forth in longitude due to their mutual repulsion as in Fig. 4, and this has not been observed. A detailed study of the SEB concluded that it was "not dynamically tied to any anticyclone vortex" (Morales-Juberias et al. 2002). Another problem with identifying Jovian vortices is that some vortices have been labeled as ephemeral, in contrast to long-lived, based on the morphologies of their associated clouds. This has led to controversy over whether long-lived Jovian cyclones exist. We have argued that they do because the long-lived Jovian anticyclones would have merged together unless they were part of a JVS, which requires cyclones (Marcus 1993), and we showed by simulating Jovian clouds that classifying a vortex as long-lived or ephemeral based on its cloud's morphology can be deceiving (Marcus 2004). There are large uncertainties in measuring the areas and potential vorticities of Jovian vortices. To find directly the potential vorticity requires differentiating velocity, which amplifies the uncertainties in the data. The area of a Jovian vortex is the area of its anomalous potential vorticity, which is the area circumscribed by the vortex's closed streamline with maximum velocity, and that is also difficult to measure. We argued (Marcus 2004) that for anticyclones, but not for cyclones, an indirect measure of the upper bound of the area of a Jovian vortex is the area of its associated cloud cover and that the aspect ratio of a vortex's north–south to east–west axes is the

best indicator of the ratio of its potential vorticity to its ambient zonal shear (Marcus 1993). However, in our opinion, all of these measurements have too much uncertainty to catalog quantitatively the areas and potential vorticities of the Jovian vortices. For this reason we focus on the qualitative features of JVSs and use the simplest equations and models.

f. No JVS contains the Great Red Spot

We view JVS as the fundamental configuration of long-lived Jovian vortices, with the GRS as the exception that proves the rule. We believe that no vortices lie within ±15° of the equator, so anticyclones at the latitude of the GRS (whose northern edge is ~15°S) have no companion cyclones on their northern sides to block their mergers with the GRS. Thus, only the GRS remains at its latitude. Presumably, the lack of long-lived vortices near the equator is because the Coriolis parameter is weak there, and a large Coriolis parameter is needed to make the flow approximately two-dimensional. (Vortices thrive in two dimensions but are quickly destroyed in three.)

3. Equations and approximations

Following Ingersoll and Cuong (1981), we model the Jovian weather layer with a one-and-a-half layer quasi-geostrophic (QG) model with no dissipation or forcing:

$$\frac{Dq}{Dt} \equiv \left[\frac{\partial}{\partial t} + (\mathbf{v}\cdot\boldsymbol{\nabla}_\perp)\right] q(x, y, t) = 0, \tag{2}$$

where the potential vorticity q is

$$q \equiv \nabla_\perp^2\psi - \frac{\psi}{L_R^2} + \beta y, \tag{3}$$

with streamfunction ψ, two-dimensional velocity $\mathbf{v} \equiv \hat{\mathbf{z}} \times \boldsymbol{\nabla}_\perp\psi$, two-dimensional gradient $\boldsymbol{\nabla}_\perp$, vertical vorticity $\omega \equiv \nabla_\perp^2\psi$, north–south gradient of the Coriolis parameter β, local vertical unit vector $\hat{\mathbf{z}}$, and local Cartesian east–west and north–south coordinates x and y, respectively. To simplify further the analyses, we let the time- and meridionally averaged zonal velocity $\overline{\mathbf{v}}(y)$ over the latitudes of a JVS have uniform potential vorticity; that is, $d^2\overline{\psi}(y)/dy^2 - \overline{\psi}(y)/L_R^2 + \beta y$ is constant, where $\overline{\psi}$ is the streamfunction of $\overline{\mathbf{v}}$. Without loss of generality the value of this potential vorticity can be set to zero (i.e., $\overline{q} \equiv 0$). The assumption that the potential vorticity of $\overline{\mathbf{v}}$ is uniform is consistent with the discussion in section 2a and with others who modeled the potential vorticity of planetary zonal flows as piecewise constant (Polvani et al. 1990; Cho et al. 2001). With this assumption, we model the local zonal velocity of a JVS (centered at a westward jet) as

$$\overline{\mathbf{v}}(y) = \left[V_0 \cosh\left(\frac{y}{L_R}\right) - \beta L_R^2\right]\hat{\mathbf{x}}, \tag{4}$$

where V_0 is an integration constant, and $y = 0$ is the latitude of the maximum of the westward jet stream. If a bottom topography were included (cf. Dowling and Ingersoll 1988) in the definition of potential vorticity in Eq. (3), then any zonal flow $\overline{\mathbf{v}}(y)$, including the one in Fig. 1, could have uniform potential vorticity if the correct bottom topography were used. In any case, our main numerical results are insensitive to the bottom topography, so we set it to zero in this paper. The westward jet at 40°S is well approximated by modeling $\overline{\mathbf{v}}(y)$ in Eq. (4) with $V_0 = 8.0\ \mathrm{m\ s^{-1}}$ and $L_R = 1400$ km. This value of L_R is corroborated by the well-measured value, $L_R = 2250 \pm 500$ km at 23°S (Marcus 1993) and the assumption that $L_R \propto 1/|\sin\lambda|$, where λ is latitude.

Equation (2) conserves energy, which up to a constant (and using $\overline{q} \equiv 0$) is

$$\begin{aligned} E &\equiv -\int\int q\,(\psi - \overline{\psi})/2\,dx\,dy - \int\int q\,\overline{\psi}\,dx\,dy \\ &= -\int\int q\,(\overline{\psi} + \psi)/2\,dx\,dy, \end{aligned} \tag{5}$$

where the integrals are over the entire domain. This energy and all other energies discussed in this paper are per unit mass surface density. To apply the energies to the Jovian weather layer they need to be multiplied by the product of the average mass density of the layer and its vertical scale height. Also conserved are the momentum in the x direction, which up to a constant is $P \equiv \int\int yq\,dx\,dy$, and the infinite moments of the enstrophy, $M_n \equiv \int\int q^n\,dx\,dy$, for nonnegative integers n. In addition to our assumption that the JVSs have piecewise-constant potential vorticity, we further simplify our model by assuming that there are $N/2$ anticyclones with potential vorticity q on the southern side of the westward jet stream and $N/2$ cyclones with potential vorticity $-q$ on the northern side (adopting the point of view of the Southern Hemisphere and $q > 0$.) With this model JVS, Eq. (2) conserves the value of the potential vorticity $\pm q$ and the areas of each vortex, A_k, $k = 1, 2, \ldots, N$, making the conservation of the moments of the potential vorticity M_n trivial. To compare calculations to observations, we work with the conserved quantity W, the width of the JVS (see Fig. 4), which is defined as the average distance between the latitude of the centers

of the anticyclones and the latitude of the centers of the cyclones. In terms of P,

$$W \equiv -2P \Big/ |q| \sum_{k=1}^{N} A_k = -2 \sum_{k=1}^{N} y_k w_k e_k, \qquad (6)$$

where e_k is 1 for an anticyclone and -1 for a cyclone, $y_k \equiv \iint_k y\, dx\, dy/A_k$ is the average latitude of the kth vortex, and $w_k \equiv A_k/\Sigma_{k'=1}^{N} A_{k'}$ is the kth weighting function (and where the integrals defining w_k and y_k are taken over the area of the kth vortex). For example, if all vortices in a JVS have the same area, then w_k is equal to $1/N$ for all k. If, in addition, each cyclone's average latitude were y_C and each anticyclone's were y_A, then the width W is equal to $(y_C - y_A)$.

In summary, the equations of motion conserve $(N + 4)$ independent quantities in our idealized JVS: energy E, width W, potential vorticity q, number of vortices N, and vortex areas A_k, $k = 1, 2, \ldots, N$.

4. Equilibrium Jovian vortex streets with no forcing and no dissipation

For the remainder of this paper, unless otherwise stated, all numerical calculations and figures use parameter values appropriate to the westward jet near 40°S., so the zonal flow $\bar{\mathbf{v}}(y)$ in Eq. (4) has $V_0 = 8.0$ m s^{-1} and $L_R = 1400$ km (see section 3). As stated in the introduction, we are not trying to model the details of the Jovian vortices, so in the calculations that follow we generically set their potential vorticities to $\pm 7 \times 10^{-6}$ s^{-1}, which underestimates the strengths of the anticyclones near 40°S (see section 2a). The calculations use an east–west domain length of 288 000 km and $N = 24$.

a. Steady JVS

Here we compute families of steady JVSs such that all of the vortex areas are the same; that is, $A_k = A$ for all k. For fixed zonal velocity $\bar{\mathbf{v}}$ and east–west or streetwise domain size, each steady JVS is uniquely determined by four quantities: its area A, width W, N and potential vorticity strength $\pm q$. (Although energy E is an independently conserved quantity, once A, W, N, and q are chosen, the E of the steady state is uniquely determined.) Therefore each steady state is uniquely characterized by L the domain size in x, the two parameters V_0 and L_R of the zonal flow $\bar{\mathbf{v}}$, and four parameters of the vortex street. In dimensionless units, the equilibria are uniquely determined by L/L_R, A/L_R^2, W/L_R, qL_R/V_0, and N. Note that even though the calculations are on a β plane, the value of β never enters—see below. To compute the steady JVSs and their eigenmodes, we use the exponentially accurate, contour-dynamics method of Van Buskirk and Marcus (1994), which computes the locations of the vortex boundaries using a continuation method, which not only produces equilibria but also determines bifurcations so we can determine stability. The method is much more economical than traditional second- or third-order accurate contour dynamics methods that are based on approximating sections of the boundary with low-order polynomials. Typically, our steady-state calculations use 64 spectral basis functions to represent the vortex boundary and our time-dependent calculations use 1024. The computational domain is unbounded in y and periodic in x.

Our goal is to determine the quasigeostrophic physics that sets W and A (since we believe that the values of q and V_0 are determined by ageostrophic forcing and are therefore beyond the scope of this paper.) Therefore, we hold qL_R/V_0, N, and L/L_R fixed (at their observed Jovian values, given in the first paragraph of this section), and compute steady solutions to Eq. (2) as functions of A/L_R^2 and W/L_R. Because the areas of all the vortices are the same, without loss of generality in a steady-state calculation, we can set $N = 2$ rather than 24, and use 1/12 the streetwise or east–west domain L to compute the steady vortex streets. We can do this because each cyclonic/anticyclonic pair of vortices is identical and they are equally spaced, so the flow has periodicity length $L/12$. Solutions that translate uniformly in x are considered steady. Results are presented in the rest frame of the vortices. The value of β only affects the value of the translation velocity, so it is irrelevant. Figure 5 shows the values of A/L_R^2 and W/L_R for which there are steady solutions. We classify JVS solutions according to their streamlines. In Fig. 3 each vortex has nested closed streamlines both within it and immediately surrounding it. The closed streamline farthest from the vortex is labeled the outermost closed streamline (OCS). Each OCS has one, two or three stagnation points lying on it. We classify JVSs as type I, II, and III in accord with the number of stagnation points on their OCS. Type III JVSs occupy only a line in A–W parameter space and separate type I's from type II's. Type II JVSs have westward-going jet streamlines that travel around the whole planet and separate the cyclones from the anticyclones. The unique westward jet streamline in type III is pinched off by stagnation points. Although a type I JVS does not have a set of uninterrupted, westward-going streamlines, the azimuthal-average (similar to the averaging-method used to create Fig. 1) of its east–west flow shows a strong westward jet

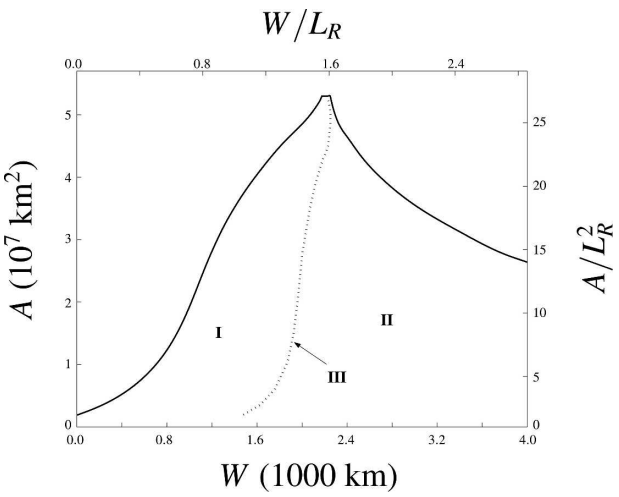

FIG. 5. Region in A–W space where JVSs exist. Parameter values are as in section 4. Steady solutions exist only between the horizontal axis with $A = 0$ and the upper curve $A_{\max}(W)$. The two-parameter families of type I (small W) JVS solutions and of type II (large W) solutions are separated by the type III solutions. The latter occupy a one-dimensional (dotted) line rather than an area. Almost all JVSs have neutral linear stability. The values of W for the type III JVS are much less than 5×10^3 km, which is the distance between the eastward jet stream at 44°S and the westward jet stream at 40°S, which bound the anticyclones in the JVS in the southern part of Fig. 2.

stream at the midlatitudes of the JVS. Figure 5 shows that steady JVS solutions have a finite range in A as a function of W, with $0 \le A \le A_{\max}(W)$. The vortices at the boundary $A = A_{\max}(W)$ fill their OCS. The physics that determines the value of $A_{\max}(W)$ for small W (type I) is the fact that vortices (whose centroids always lie in regions where the ambient shear has the same sign as the potential vorticity of the vortex) cannot extend far into regions where the shear has the opposite sign. This means that a vortex's boundary cannot extend very far across the latitude $y = 0$. Therefore vortices in a street with small W must have small areas, and their maximum size increases with W, so $A_{\max}(W)$ increases with W. For large W (type II), the physics that determines the maximum size of the vortex is the fact that a vortex cannot extend very far into regions where the shear has the same sign as the potential vorticity, but with much greater magnitude. (When the shear becomes large it stretches the vortex too much for it to have an equilibrium.) For large W streets, as W increases the magnitude of the ambient shear of the side of the OCS that is farthest from $y = 0$ increases exponentially with W. Therefore for type II vortices as W increases, the maximum size of the vortex decreases, and $A_{\max}(W)$ decreases with W. Type II and III steady JVSs are neutrally stable. Type I's are neutrally stable except[1] for a small region of instability where $A \gtrsim 0.95\, A_{\max}(W)$.

b. Time-dependent, oscillating JVS

A steady-state JVS has $N/2$ eigenmodes, but we are interested in the primary mode, defined here to be the mode where the orbits of the centroids (here, centroid is defined as the center of the potential vorticity) of the cyclones are all in phase and 180° out of phase with those of the anticyclones. A finite-amplitude extension of this eigenmode is shown in Fig. 4. It can be created by displacing all of the vortices in a steady JVS north by a distance Δy. When thus initialized, each vortex executes an elongated orbit about its original, unperturbed location with a north–south semidiameter or amplitude equal to Δy. This time-dependent JVS and the steady JVS from which it was perturbed, hereafter defined to be its reference JVS, have the same values of N, q, A, and W because the perturbation, regardless of the size of Δy, conserves them exactly. A cyclone and anticyclone in a JVS at latitudes $(y_C + \Delta y)$ and $(y_A + \Delta y)$ (and several L_R away from each other) will approach each other with a collisional east–west velocity

$$|V_{\rm Col}| \equiv |\overline{\mathbf{v}}(y_C + \Delta y) - \overline{\mathbf{v}}(y_A + \Delta y)| \simeq 2\overline{\sigma}_{AC}\Delta y, \quad (7)$$

where y_A and y_C are the latitudes of the vortices in the reference JVS, where we used the fact that $[\overline{\mathbf{v}}(y_C) - \overline{\mathbf{v}}(y_A)] = 0$ because the reference JVS is steady, and where $\overline{\sigma}_{AC} \equiv |\overline{\sigma}(y_A) - \overline{\sigma}(y_C)|/2$, which is the average absolute value of the shear at the centers of all of the vortices in the reference JVS. The approximate temporal period of the primary mode is a function of $|V_{\rm Col}|$ and of the east–west diameter of its orbit (which for a vortex street on Jupiter consisting of N vortices is $\sim 2\pi R_J/N$). We define the period

$$\tau \equiv 4\pi R_J/N|V_{\rm Col}| \simeq 2\pi R_J/N\overline{\sigma}_{AC}\Delta y. \quad (8)$$

[1] For fixed W/L_R, the primary family of steady JVS solutions begins at $A = 0$ and terminates at $A = A_{\max}(W)$. For a JVS with $A = A_{\max}$, the vortex boundaries have cusps (because they lie on an OCS containing a stagnation point). For most values of W/L_R in Fig. 5, there are no secondary branches of steady JVS solutions that intersect the primary branch. However, for some small range of W/L_R (corresponding to the location in phase space where there are nonneutral instabilities), the type I JVS primary branch of solutions has a forward pitchfork bifurcation for values of A greater than $0.95\, A_{\max}(W)$, which causes the primary branch to become unstable. Despite the mathematical curiosities associated with vortices with cusps, the secondary branch of JVS solutions, and the instabilities, these phenomena are not relevant to Jovian vortices (whose photographs may show filamentation, but never cusps). As shown in section 6, the ambient turbulence prevents the vortex areas from getting close to $A_{\max}(W)$.

This estimate of the period τ as a function of north–south oscillation amplitude Δy and shear $\overline{\sigma}$, as well as the relations among these quantities and the east–west orbital velocity V_{Col}, given by Eqs. (1) and (7) agree well with our numerically computed JVS and are also consistent with observations of the White Ovals (Rogers and Herbert 1991; also see Rogers 1995, his Figs. 11.9–11.11, p. 225). Although τ, V_{Col}, and Δy are useful observational measures for Jovian vortex streets, a more useful theoretical measure is the difference in energy ΔE between a JVS and its reference JVS. The $|\Delta E|$ for a JVS (per cyclone/anticyclone pair, so a street on Jupiter with 12 pairs of vortices would have 12 times this energy) is related to Δy by

$$|\Delta E| \simeq qA\overline{\sigma}_{AC}(\Delta y)^2 = qA(V_{\mathrm{Col}})^2/4\overline{\sigma}_{AC} = 4\pi^2 qA(R_J)^2/N^2\tau^2\overline{\sigma}_{AC}. \quad (9)$$

Equation (9) follows from Eq. (5), by noting that when every vortex of a steady JVS is displaced by Δy, the term $\iint q(\psi - \overline{\psi})/2\, dx\, dy$ in Eq. (5) is unchanged[2] and that for a vortex centered at latitude y_i, $\iint q\,\overline{\psi}\, dx\, dy \simeq qA\overline{\psi}(y_i)$, so $\Delta E \simeq -qA\{[\overline{\psi}(y_A + \Delta y) - \overline{\psi}(y_A)] - [\overline{\psi}(y_C + \Delta y) - \overline{\psi}(y_C)]\}$. Taylor expanding $\overline{\psi}$ in this last expression[3] and using $[\overline{\mathbf{v}}(y_C) - \overline{\mathbf{v}}(y_A)] \equiv 0$ and $\overline{\sigma}(y_C) = -\overline{\sigma}(y_A) = \overline{\sigma}_{AC}$, gives Eq. (9).

Thus to characterize a time-dependent JVS (that either has $N = 2$ or only has only its primary mode excited) we need to not only specify its area A, number of vortices N, width W, and potential vorticity q, but also any one of the following: the north–south amplitude of its oscillation Δy, the east–west velocity of its elongated orbit V_{Col}, its period τ, or its energy difference ΔE with respect to its reference JVS. (The cyclones and anticyclones in Jupiter's vortex streets have areas and absolute values of their potential vorticities that are not the same. However Eqs. (7)–(9) are still valid, if q, A, and Δy are defined as the potential vorticities, areas, and north–south oscillation amplitudes of the elongated orbits of the anticyclones, and if we define $\overline{\sigma}_{AC} \equiv [\overline{\sigma}(y_A) - \overline{\sigma}(y_C)(A/A_C)|q/q_C|]/2$, where A_C and q_C are the areas and potential vorticities of the cyclones. The amplitude of the north–south oscillations of the cyclones is $(A/A_C)|q/q_C|\Delta y$, so momentum and width W are conserved.

[2] Here, $(\psi - \overline{\psi})$ is the streamfunction due to the vortices only, so is invariant under translation of the ensemble of vortices in any direction; similarly, q is invariant when $\overline{q} = 0$.

[3] The first three terms in the Taylor expansion of $\overline{\psi}(y_C + \Delta y)$ are $\overline{\psi}(y_C) + (\Delta y)d\overline{\psi}/dy|_{y_C} + [(\Delta y)^2/2]d^2\overline{\psi}/dy^2|_{y_C} = \overline{\psi}(y_C) - (\Delta y)\overline{\mathbf{v}}(y_C) + [(\Delta y)^2/2]\overline{\sigma}(y_C)$.

5. New model of forcing and dissipation

a. Traditional models and their inadequacies

Because JVSs are neutrally stable for a wide range of A and W, existence or stability cannot select the values of A and W on Jupiter. For this reason, we consider forcing and dissipation. In geophysical fluid dynamics, dissipation is traditionally modeled with a hyperviscosity, which damps the smallest spatial scales (Pouquet et al. 1975). Hyperviscosity works well for studies of vortex dynamics in part because the time scale of vortex interactions is the vortex turn-around time. Typical simulations require at most a few hundred turn-around times, and for these durations the amount of dissipation in the physically important spatial scales is not significant. Hyperviscosity also works well for simulations which focus on producing large-scale structures, such as zonal flows, via inverse energy cascades from small-scale forcing (Vallis and Maltrud 1993; Panetta 1993; Danilov and Gryanik 2004). Although these simulations often run for several thousand turn-around times, hyperviscosity can be used because most of the late-time energy resides in the nearly dissipationless large scales, and the details of the small scales are unimportant. In 2D calculations, the forcing effects from the unresolved or uncalculated ageostrophic and 3D motions such as plumes rising from lower layers or baroclinic instabilities are often modeled by forcing the vertical component of vorticity either in wavenumber space or physical space. Figure 6 illustrates the problems of using hyperviscosity in this study of JVSs, which, as we show in section 6, requires the faithful simulation of the small scales in the vortex filaments and boundaries over several thousand vortex turn-around times. The evolution of the White Ovals took place over 60 yr, or ~3000 turn-around times, which is comparable to the number of turn-around times (~5000) that the JVS in Fig. 6 required to come to a statistically steady state. Figure 6 shows two calculations in which a JVSs is evolved with hyperviscosity and forcing. (See caption for computational details.) Although the initial JVSs in the two calculations are different, at late times they are nearly the same. Both calculations have $N = 2$ and have the same values of q, L_R, and $\overline{\mathbf{v}}(y)$, and the same forcing and dissipation. Figure 6 shows that the width W of each JVS evolves in time, with the small W increasing and the large W decreasing. Figure 7 shows the evolution of these two JVS in the A–W plane. They appear to have a common attractor. This suggests that our forcing and dissipation models select a unique A and W. However, over these long time scales' hyperviscosity washes out the filaments, as well as the sharp gradients of po-

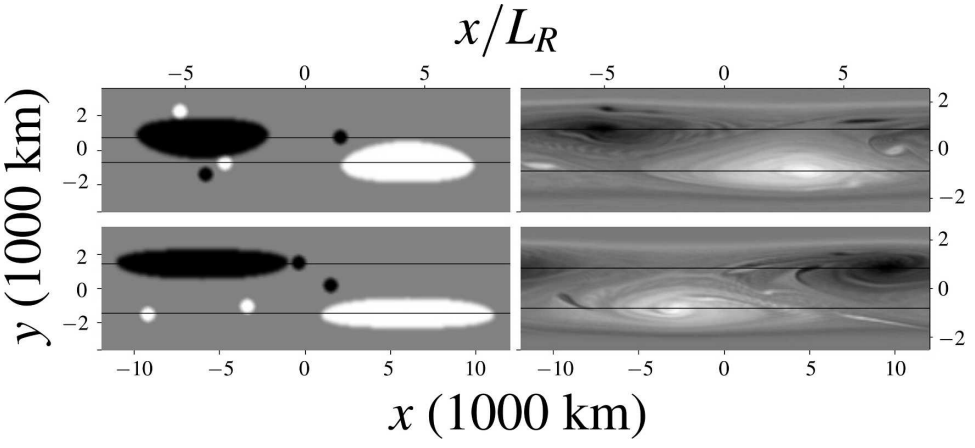

FIG. 6. Calculation with traditional forcing and hyperviscous dissipation of two initially different JVSs. Parameter values are as in section 4. (top left) A grayscale shows the potential vorticity of an initial $N = 2$ JVS (the two large vortices with $\pm q$). Initially, $A/L_R^2 = 7.2$ and the width W is small, $W/L_R = 0.99$. The flow is forced by adding opposite-signed pairs of small vortices randomly in space and periodically in time (approximately two pairs per turn-around time of a large vortex). The small vortices have the same strength potential vorticities as the initial vortices in the JVS, and their areas are ~0.03 times that of the initial large vortices. The solid horizontal lines in each panel are the latitudes of the centroids of the large vortices. (top right) The same flow after being forced and dissipated for ~5000 turn-around times. Although W has increased, the details of the vortex structures, e.g., its filaments, have been washed out. (bottom) Similar to (top) but showing an initial JVS with a $A/L_R^2 = 6.7$ and a larger W, $W/L_R = 2.1$. W decreases in time. The doubly periodic spectral calculations have 256×512 collocation points. A fourfold increase in spatial resolution postpones the time at which the boundaries and filaments first become poorly resolved, but, nonetheless, they are always washed out by the time the JVS approaches its attractor.

tential vorticity at the vortex boundaries, making the existence of an attractor uncertain and, in any case, making it impossible to deduce the physics that drives the flow to its late-time state.

b. New model

1) DISSIPATION

Because our model of forcing and dissipation is novel, we want the effects of the model on the late-time JVS to depend only on the model's physically motivated rules and not on the numerical contrivances needed to compute them such as the vagaries of a poorly understood numerical grid-viscosity, hyperviscosity or underresolved spatial discretization. We require a numerical method that preserves sharp vortex boundaries (because that is a property of vortices embedded in a shear) and resolves filamentation (because *Voyager* movies show frequent filamentations, and simulations in section 5a suggest they are important). For these reasons we choose a model that can be computed with contour dynamics, which, by using the spectral implementation of Van Buskirk and Marcus (1994), has effectively no numerical dissipation. Unlike unembedded vortices that continually filament and require the highly dissipative numerical artifact of contour surgery, vortices embedded in a JVS shed filaments only when they encounter stagnation points (section 2a), minimizing the need for contour surgery. Like Dritschel (1989), we found that the flow is insensitive to

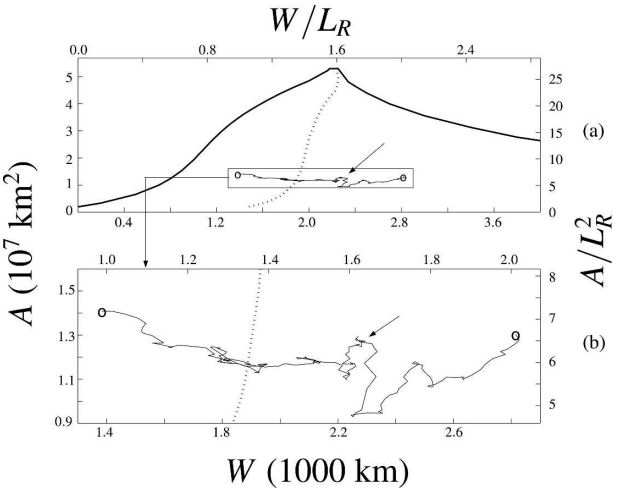

FIG. 7. Evolution in the A–W plane of the two JVSs in Fig. 6. (a) Two initial conditions (open circles) evolve toward their common attractor near the locus of type III JVSs (dotted line). (b) Blow-up showing the details within the rectangular box in (a) and illustrating the late-time attracting JVS where the two evolutionary tracks cross (arrow).

the choice of the thinness criterion for removing the filament. Dissipation via contour surgery conserves the potential vorticities q and N of a JVS but changes its width W, area A, and energy. When a filament with centroid at latitude y_f and area a is removed from a vortex, the momentum P changes by $\delta P \simeq -qay_f$ and width W changes by

$$\delta W = \pm 2ay_f \Big/ \left(\sum_{k=1}^{N} A_k \right), \tag{10}$$

where the sign is positive (negative) for anticyclones (cyclones).

2) FORCING

Repeatedly adding small vortices to the flow and computing their mergers as we did in the traditional forcing calculations in Fig. 6 quickly becomes intractable with a contour dynamics calculation. Therefore, instead of computing mergers, we model their effects. We self-similarly expand the area of each large vortex in the JVS, keeping its shape, centroid (and therefore its latitude y_k) and potential vorticity q unchanged. Therefore the width W of the JVS is unchanged. We keep q unchanged because we assume, as in section 5a, that the small vortices of the forcing have potential vorticities $\pm q$. Our motivation for keeping the centroids constant is that we found that it was approximately true in the simulations in section 5a because the small vortices appended themselves to the larges vortices at approximately random locations along their boundaries. In testing our forcing model, we varied the rate at which the forcing increased the areas of the vortices and found that the rate had little effect on the properties of the attracting JVS, but did determine how fast the flow evolved to it. For the remainder of the paper we use a rate of increase of $0.028L_R^2$ per average oscillation period τ as defined in Eq. (8). To get a physical understanding of this rate, note that if a Jovian anticyclone at 41°S expanded at this rate (and never filamented), its area would increase by ~0.7% per τ. With this forcing, the vortices shed filaments as they encounter stagnation points, but the amplitudes of the oscillations in their elongated orbits run down; the east–west velocity V_{Col} of the oscillation, its north–south amplitude Δy, and the energy difference $|\Delta E|$ between the JVS and its reference JVS decrease to zero. Each JVS evolves toward the $A_{\max}(W)$ curve in Fig. 5 and then moves along or near the $A_{\max}(W)$ curve until it come to the region near the type III JVS where it remains. This behavior is inconsistent both with our simulations using traditional forcing and dissipation (Fig. 7) and with Jupiter where the oscillations of the JVS do not run down. The inconsistency is due to the fact that the small vortices used in traditional forcing bump and displace the large vortices as they merge, preventing Δy, $|\Delta E|$, and V_{Col} from decaying to zero. Our calculations with traditional forcing suggest (but not definitively, due to hyperviscosity) that ΔE remains approximately constant as the flow evolves. To model this effect of the atmospheric turbulence, we added a second component to the forcing to maintain a constant value of ΔE by continually adding very small random displacements to the individual vortices (subject to the constraint that the momentum, or equivalently W, was unchanged). Numerical experiments showed that all of the different types of displacements we tried led to the same result. Therefore for simplicity, we did the following: at fixed phases in the JVS oscillation we shifted the latitudes of all the vortices in the JVS by the same amount while keeping their longitudes constant. This shift conserves A, W, q, and N, and changes ΔE in accord with Eq. (9). The magnitude of the shift was chosen to keep $|\Delta E|$ constant throughout the calculation. By shifting the latitudes of the vortices, we put energy into the system and cause the vortices to oscillate about the equilibrium (reference JVS). Shifting the latitudes of all of the vortices corresponds to changing the energy of the primary eigenmode of the JVS (see section 2d and Fig. 4). The shifts in latitude are so small that the cumulative shift in a calculation from start to finish is always much smaller than either the width W of the JVS or the diameters of the vortices. The power supplied by our forcing is also small; it is less than 0.1% of the power equal to the product of the flux of the Jovian internal heat flux (~5.4 W m^{-2}) and the area of an anticyclone in the JVS. A practical calculational advantage of shifting the latitudes of all of the vortices simultaneously, is that we can limit our study[4] to JVS with $N = 2$. Thus for the remainder of the article we set $N = 2$. The value of ΔE can be thought of as a parameterization of the strength of the ambient turbulence. In summary, our forcing model consists of two parts. The first is an increase in area of all the vortices, while holding width W, potential vorticity q and N fixed, and a second part that maintains a constant value of ΔE fixed while holding area A, width W, potential vorticity q, and N fixed.

[4] With this forcing, the reference JVS, the damping and forcing are identical for each cyclone/anticyclone pair, so even though the computation with N vortices is periodic in the east–west direction with periodicity length L, the flow has periodicity length $2L/N$, so we can limit the calculation to only one pair of vortices in the smaller computational domain, provided that the calculations with $N = 2$ vortices have no subharmonic instabilities.

6. Evolution to an attractor with the new model of forcing and dissipation

The evolutions of the two JVSs in the A–W plane in Fig. 8 are typical of initial-value runs with the new forcing and dissipation. There is a common attractor for initial conditions with the same values of N, q, L_R, $\overline{\mathbf{v}}(y)$, and forcing amplitude ΔE. We now explain why the attractor in our calculations always has a value of width W that is approximately equal to that of the steady type III JVS with the same area A as the attracting solution. We also show that the width W of the attractor is independent of the details of the forcing model but that its area A depends on the forcing amplitude ΔE.

a. Change in W due to filamentation

The outermost closed streamlines (OCS) determine how W changes. Figure 9a shows a filament shedding from an anticyclone on the southern side of a type I JVS with streamlines similar to Fig. 3a. The portion of the vortex that overflows the OCS is carried counterclockwise around the anticyclone to the stagnation point to its north. From there it is stretched into a filament and swept north across the westward-going jet stream (at $y \equiv 0$), so the filament's centroid has $y_f > 0$. Before clipping, filamentation conserves momentum $P \equiv \iint yq\, dx\, dy$, so as the filament moves north, the body of the vortex recoils south. When the filament is clipped, the width W increases (i.e., $\delta W > 0$), consistent with Eq. (10) because $y_f > 0$ and $q > 0$. Due to the locations of the stagnation points on the OCS, both the anticyclones and cyclones in a type I JVS, always shed their filaments on the opposite side of the street (i.e., on the other side of the westward jet stream) of the vortex from which they came, causing the JVS to widen. In contrast, Fig. 9b shows a type II JVS shedding filaments on the same side of the street, causing the width W to narrow. A type II JVS has streamlines similar to Fig. 3b. Each vortex has two stagnation points on its OCS from which it can shed filaments. However, simulations show that the southern vortex (an anticyclone) in Fig. 9b usually overflows the segment of OCS on its southern side because that segment of OCS is closer to the vortex than its northern segment. The portion of the vortex that overflows is carried counterclockwise around the vortex to the stagnation point on its eastern side where it is swept south of the JVS, causing the body of the vortex to recoil north. When the filament is clipped, $y_f < 0$, which causes the width W to decrease in accord with Eq. (10). Only rarely does a type II JVS filament to the opposite side of the street as in Fig. 9c. When it does, y_f and δW are very small and of either sign. Figures 10 and 11 summarize filamentation. Each

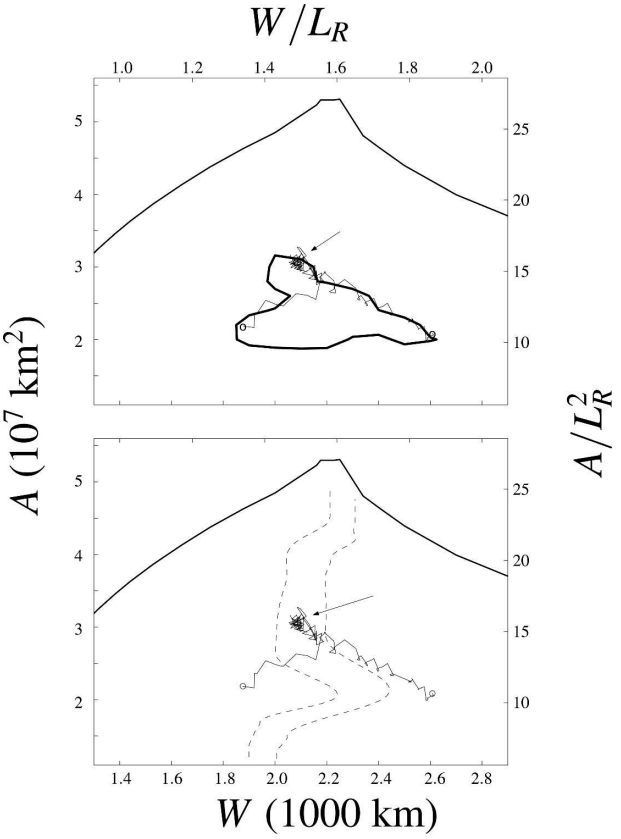

FIG. 8. Evolution in the A–W plane of an initially narrow and of an initially wide JVS computed with the new forcing model with $|\Delta E| = 70$. Initial locations are shown as open circles. Parameter values are the same as in section 4. (a) Both flows evolve to the same late-time JVS (denoted by arrow). The heavy closed curve is the contour for $E_{\text{crit}} = 70$; the evolutionary paths of the two JVSs are nearly coincident with it. The late-time flow is not steady, but meanders around a fixed point due to its never-ending cycle of shedding finite-sized filaments and increasing its area. (b) Same as (a), but showing the two broken curves bounding W-attracting region described in Fig. 10 rather than an energy contour.

symbol in Fig. 10 was computed by beginning with a steady JVS with the area A and width W of the symbol's position in the A–W plane. We then increased $|\Delta E|$ from zero (holding A and W constant) by shifting the JVS north or south, causing the vortices to oscillate. We increased $|\Delta E|$ to the critical value $E_{\text{crit}}(A, W)$ where the vortices first shed filaments. Figure 11 shows contours of constant $E_{\text{crit}}(A, W)$ in the A–W plane. Each arrowhead in Fig. 10 points to the direction (wider or narrower W) that the filamentation drives the JVS. Open circles indicate a small δW caused usually by a type II vortex filamenting to the opposite side of the street as in Fig. 9c. Thus filamentation, not the forcing model, causes JVSs to be attracted to the region in the A–W plane between the two broken curves in Fig. 10 (near the type III JVS). This W-attracting region is con-

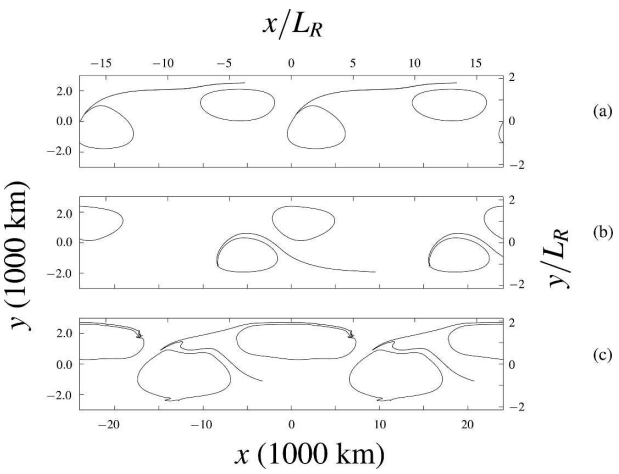

FIG. 9. Calculation of filaments shed from vortices near stagnation points. The filament and the body of the vortex from which it is shed move in opposite directions in latitude, so the width W of the JVS changes when the filament is clipped. (a) Type I JVS [with parameter values of the reference JVS (Fig. 3a), but not steady because the vortices are initially displaced north]. The streamlines in Figs. 3a and 9a are similar but the latter are time dependent. The filament is shed and clipped on the opposite side of the vortex street of the vortex that shed it, thereby increasing W. (b) Type II JVS. (The initial condition is created by displacing the reference JVS in Fig. 3b north.) The vortex overflows its closer, southern segment of OCS. The filament is shed and clipped on the same side of the vortex street, decreasing W. (c) Type II JVS (the initial condition is created by displacing a reference JVS with $W = 2000$ km and $A = 2.4 \times 10^7$ km^2 north—see open circle in Fig. 10). This is the rare case when a vortex overflows the far segment of its OCS. The shed filament becomes entangled with the westward jet stream and the southern vortices, causing a δW of either sign.

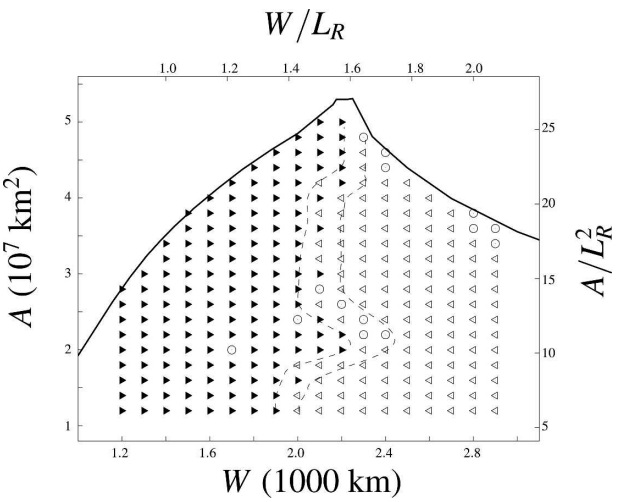

FIG. 10. W-attracting region and the change in W due to filamentation. Parameter values are as in section 4. Each symbol represents a numerical experiment. Each began with the steady reference JVS for the A and W indicated by the location of the symbol. $|\Delta E|$ was increased until it reached a critical value E_{crit} and a filament was shed. Arrowheads pointing to the right (left) indicate that the filamentation increased (decreased) W after the filament was clipped. Circles represent experiments in which δW was small. The two broken curves are to guide the eye. They are our best estimate (based on the circles and arrowheads) of the bounds of the W-attracting region to which all JVS are drawn due to filamentation.

sistent with the attractors in initial-value calculations run either with traditional forcing and dissipation (Fig. 6) or our new model (Fig. 8).

b. Slow evolution along contours of $E_{crit}(A, W)$

Figure 8 shows two JVSs evolving with our forcing model with $|\Delta E| = 70$. Both JVSs zig-zag along the contour $E_{crit}(A, W) = |\Delta E| = 70$. The value of $|\Delta E| = 70$ is our choice of forcing for this calculation, whereas $E_{crit}(A, W)$ is a property of the JVS and independent of the forcing intensity. At late times, our simulations always show that JVSs follow the branches of contours of $E_{crit}(A, W) = |\Delta E|$ with $\partial E_{crit}/\partial A < 0$ [i.e., the large-area (upper) branch of the closed contour in Fig. 8a]. We refer to this branch as the attracting branch. Once the JVS enters the W-attracting region, it remains there indefinitely. Thus, the intensity of the forcing $|\Delta E|$ determines the area A of the attractor. To understand the slow evolution of a JVS along the attracting branch, consider the case where the initial JVS lies on the branch. The first part of our forcing model increases the area A. However, $\partial E_{crit}/\partial A < 0$, so this increase in area decreases E_{crit} below the imposed ΔE. Thus, the vortices shed filaments, decreasing A and changing the width W in accord with Fig. 10. The decrease in area A returns the JVS to its attracting branch but with a new value of W. The cycle of increase in A and filamentation repeats, and the JVS zig-zags along its attracting branch until it reaches the W-attracting region. As a JVS evolves in the A–W plane, so does its reference JVS; both of their energies change in time, but their energy difference ΔE remains approximately constant.

Now consider the evolution of a JVS that is not initially on its attracting branch and is instead located in the A–W plane interior to the closed contour with $E_{crit}(A, W) = |\Delta E|$. Inside the contour, $E_{crit}(A, W) > |\Delta E|$, so the JVS cannot shed filaments. Instead, the forcing increases its area A until it reaches the attracting branch and then evolves as in the previous case. A JVS with initial values of A and W that lie outside the closed energy contour with $E_{crit}(A, W) = |\Delta E|$ will, in general have $E_{crit}(A, W) < |\Delta E|$ [although Fig. 12 highlights a case where this is not true because the contour with $E_{crit}(A, W) = |\Delta E|$ is not unique.] Often these flows evolve to an attracting branch and end their evo-

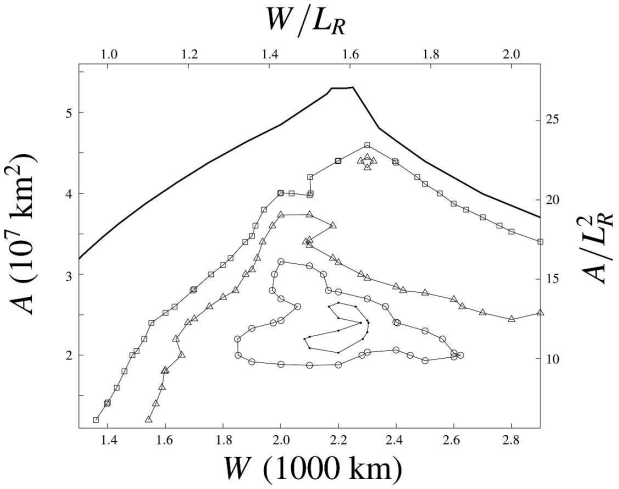

FIG. 11. $E_{crit}(A, W)$ plotted as contours in the A–W plane. Parameter values are as in section 4. The maximum area of a JVS $A_{max}(W)$ is shown as a heavy curve, and it is nearly coincident with the contour of $E_{crit} = 0$. On contours with a □, E_{crit} is 15; with a △ it is 30, with a ○ it is 70, and with no large superposed symbol is 110. Large E_{crit} means that large amplitude turbulence $|\Delta E|$ is needed to cause a JVS to shed filaments. Energies have units of $km^4\ s^{-2}$, so to apply them to Jupiter they must be multiplied by product of the average density of the weather layer and its vertical pressure scale height.

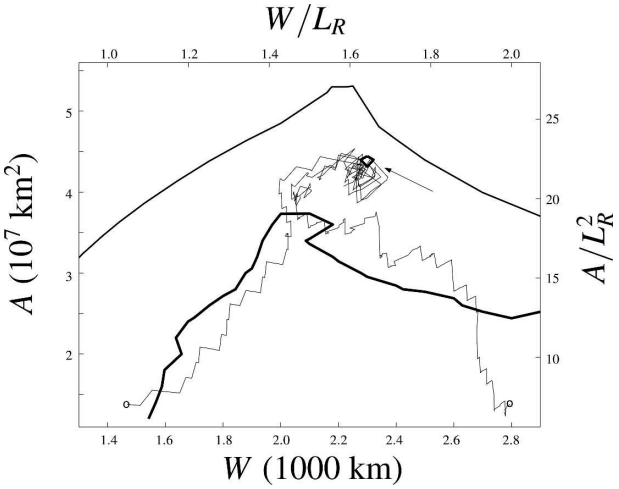

FIG. 12. Evolution of two JVSs using a forcing with $|\Delta E| = 30$. Initial locations are shown as open circles. Parameter values are the same as in section 4. (The A and W of the two initial conditions are approximately equal to those in Figs. 6 and 7. They would be identical, but the plots in Figs. 6 and 7 begin only after the very early transients, which allow the vortex shapes to adjust to their local equilibrium values, have ended.) The attracting JVS is marked with the arrow. The two distinct contours with $E_{crit} = 30$ are shown as thick curves. (See the curve denoted with triangles in Fig. 11 for additional clarity.) Initially the JVSs are attracted to and follow the lower contour. They evolve along it with large zig-zag steps, enabling them to sample large regions of the A–W plane. Once inside the W-attracting region, they jump to the small, closed contour where the attracting solution is indicated with an arrow.

lution at the attractor. However, when $|\Delta E| \gg E_{crit}(A, W)$, the vortices oscillate with large amplitude, allowing them to have close encounters with each other that frequently rip them apart and destroy the JVS. On or near the curve $A = A_{max}(W)$ in the A–W plane (where the vortices could have cusps—see section 4), E_{crit} is nearly zero, so only a very laminar JVS with $\Delta E \simeq 0$ can exist in this region. For flows with finite ΔE, the vortices in a JVS with $A \simeq A_{max}(W)$ are quickly destroyed.

Because of the finite size of the zig-zag steps taken by the JVS as it evolves, its approach to its attractor is noisy. This allows the flow to sample large regions of the A–W plane. When multiple attracting branches exist, the flow generally ends on the one with the largest area A. For example, two closed contours in Fig. 11 have $E_{crit} = 30$. Figure 12 shows the evolution of two initially-different JVSs subject to forcing with $|\Delta E| = 30$. Both initially evolve along the lower attracting branch, but once inside the W-attracting region, they jump to the branch with larger area A.

7. Conclusions and comparisons with observations

Filamentation, rather than forcing, determines the width W of the attracting Jovian vortex street (JVS). JVSs wider than that width shed filaments to the "same side of the street" as the vortices that shed them, causing the streets to narrow; JVSs with narrower widths shed filaments to the "opposite side of the street," causing them to widen. Vortices within a JVS in the W-attracting region shed filaments to both sides of the street, thereby keep their JVS within the W-attracting region. If the streamlines of the oscillating and of the steady JVS were identical, then the W-attracting region in Fig. 10 would coincide with the locus of type III JVS in Fig. 5. When there are large differences between the streamlines of the steady and oscillating JVS, there are relatively large deviations between the W-attracting region and the locus of the type III JVS. This is why the largest deviation occurs for the values of A and W in Fig. 11 where E_{crit} (and therefore the amplitude of the nonfilamenting oscillation) is greatest.

The area A of the attracting JVS is determined by the amplitude ΔE of the forcing. The attractor's area A lies at the intersection of the W-attracting region in Fig. 10 and the large-A (upper) branch of the contour with energy $E_{crit} = \Delta E$ in Fig. 11. Thus, Figs. 10 and 11, along with the value of ΔE, determine the A and W of the attracting JVS. The relation between ΔE and observables such as the amplitude of the ambient turbu-

lence could be determined if the functional form of the turbulent energy spectrum were known, but it is not. Fortunately, ΔE can be determined from observations with Eq. (9) using the period of the elongated orbit of the vortex (i.e., its oscillation period) τ, velocity of the oscillation V_{Col}, *or* the north–south amplitude δy of the elongated vortex orbits, all of which are known for the JVS containing the White Ovals (Rogers 1995) and all of which could be measured for other Jovian vortex streets. (Unfortunately, there are large uncertainties in the values of the potential vorticities and areas of the vortices.)

The fact that the intensity of the forcing determines the area A of the attractor has precedent. Van Buskirk (1991), in modeling the GRS, showed that the energy of the ambient turbulence determines the area of an isolated vortex embedded in a zonal flow with alternating jet streams. Using a continuation method to compute a family of steady embedded vortices, he found that as the area of a vortex increased so did the area circumscribed by its OCS but not as rapidly; the family of vortices ended with a maximal area vortex characterized by the vortex filling its entire OCS. Using an initial-value code, he created nearly maximal area vortices in laminar, but not turbulent, flows. He found that turbulence continually displaced a vortex, and when the displacements were as large as the distance between the vortex's boundary and its OCS, the vortex bumps the OCS and area is stripped from it. The stronger the ambient turbulence, the more frequent the bumping and stripping, and the smaller the area of the surviving vortex. The oscillation amplitude ΔE in the forcing model here, acts in a manner similar to Van Buskirk's turbulence by regulating the bumping and thereby determines the area of the attracting vortex.

Many of the key ideas developed here, such as Eqs. (7)–(9), can be tested against observations because they are valid for the more general case exemplified by Jupiter's streets in which the absolute values of the potential vorticities in the street are not all equal. Between 1945 and 1995 the areas and east–west diameters L_x of the White Ovals in the JVS at 33°S shrank; the aspect ratio $\eta \equiv L_x/L_y$ of each White Oval remained approximately constant (where L_y is the Oval's north–south diameter); and the north–south amplitude Δy of the elongated orbits of the White Ovals increased. Qualitatively, observations show that $\Delta y \propto 1/L_x$ [Figs. 11.7, 11.9, 11.11 and 11.15 of Rogers (1995)]. This is not a relationship that can be explained by a simple decay of the White Ovals. The aspect ratio of a vortex embedded in an ambient zonal shear is a measure of its potential vorticity (Marcus 1993), so the observation that the aspect ratio did not change between 1945 and 1995 suggests that the potential vorticities of the White Ovals remained constant despite their decrease in area. Equation (9), along with the fact that the area A of a White Oval is approximately equal to $\pi L_x L_y/4 = \pi(L_x)^2/4\eta$, shows that

$$\Delta y \simeq \sqrt{4\eta|\Delta E|/(\pi q\overline{\sigma}_{AC})}/L_x. \tag{11}$$

At 34°S, $\overline{\sigma}_{AC}$ is not a strong function of latitude. Therefore, if the amplitude of the forcing $|\Delta E|$ remained constant during 1945–95, then Eq. (11) explains the observation that Δy is approximately proportional to $(1/L_x)$.

Figure 2 shows that the average width W of Jupiter's vortex street at 40° is ~2000 km, in agreement with the type III JVS and the W-attracting region in Figs. 5 and 7–12, which were computed for the parameters appropriate to this JVS with the caveat that we arbitrarily set the absolute value of the potential vorticities of the anticyclones to that of the weaker cyclones. In principle, we could recompute the streamlines and stagnation points of the W-attracting region with better values of the potential vorticities and compare them to observations. However, the estimates of the potential vorticities and observations of the streamlines are fraught with uncertainties. A more compelling argument that Jupiter's vortex streets at 40° and at 33°S (before the mergers of the White Ovals) evolved to their W-attracting regions comes from the filamentation pattern of their vortices. The signature of a JVS in the W-attracting region, even when the absolute values of the potential vorticities and areas of the cyclones and anticyclones differ, is that it sheds filaments to both sides of the street. Assuming that the clouds are tracers of potential vorticity, this signature shedding has been observed for the streets at 40° and 33°S. For example, Fig. 2 shows cyclones shedding filaments to both sides of their respective streets.

Acknowledgments. We thank the NASA Planetary Atmospheres Program (NNG06GA09G) for support. Computations were run at the San Diego Supercomputer Center (NPACI, supported by NSF). One of us (PSM) also thanks the Miller Institute for Basic Research in Science for support.

REFERENCES

Barranco, J., and P. S. Marcus, 2005: Three-dimensional vortices in stratified protoplanetary disks. *Astrophys. J.,* **623,** 1157–1170.

Cho, J. Y.-K., and L. M. Polvani, 1996: The emergence of jets and vortices in freely evolving, shallow-water turbulence on a sphere. *Phys. Fluids,* **8,** 1531–1552.

——, M. de la Torre Juarez, A. P. Ingersoll, and D. G. Dritschel,

2001: High-resolution, three-dimensional model of Jupiter's Great Red Spot. *J. Geophys. Res.,* **106,** 5099–5105.

Chorin, A. J., 1997: *Vorticity and Turbulence.* Springer, 174 pp.

Danilov, S., and V. M. Gryanik, 2004: Barotropic beta-plane turbulence in a regime with strong zonal jets revisited. *J. Atmos. Sci.,* **61,** 2283–2295.

Deem, G. S., and N. J. Zabusky, 1978: Vortex waves: Stationary V states, interactions, recurrence, and breaking. *Phys. Rev. Lett.,* **40,** 859–862.

Dowling, T. E., and A. P. Ingersoll, 1988: Potential vorticity and layer thickness variations in the flow around Jupiter's Great Red Spot and White Oval BC. *J. Atmos. Sci.,* **45,** 1380–1396.

——, and ——, 1989: Jupiter's Great Red Spot as a shallow water system. *J. Atmos. Sci.,* **46,** 3256–3278.

Dritschel, D. G., 1986: The nonlinear evolution of rotating configurations of uniform vorticity. *J. Fluid Mech.,* **172,** 157–182.

——, 1988: The repeated filamentation of two-dimensional vorticity interfaces. *J. Fluid Mech.,* **194,** 511–547.

——, 1989: Contour dynamics and contour surgery: Numerical algorithms for extended, high-resolution modelling of vortex dynamics in two-dimensional, inviscid, incompressible flows. *Comput. Phys. Rep.,* **10,** 77–146.

——, 1990: The stability of elliptical vortices in an external straining flow. *J. Fluid Mech.,* **210,** 223–261.

Hook, R., 1665: A spot in one of the belts of Jupiter. *Philos. Trans.,* **1,** 3.

Ingersoll, A. P., and P. G. Cuong, 1981: Numerical model of long-lived Jovian vortices. *J. Atmos. Sci.,* **38,** 2067–2076.

Lamb, H., 1945: *Hydrodynamics.* Dover Publications, 738 pp.

Limaye, S. S., 1986: Jupiter: New estimates of the mean zonal flow at the cloud level. *Icarus,* **65,** 335–352.

MacLow, M.-M., and A. P. Ingersoll, 1986: Merging of vortices in the atmosphere of Jupiter: An analysis of Voyager images. *Icarus,* **65,** 353–369.

Marcus, P. S., 1988: Numerical simulation of Jupiter's Great Red Spot. *Nature,* **331,** 693–696.

——, 1990: Vortex dynamics a in shearing zonal flow. *J. Fluid Mech.,* **215,** 393–430.

——, 1993: Jupiter's Great Red Spot and other vortices. *Annu. Rev. Astron. Astrophys.,* **31,** 523–573.

——, 2004: Prediction of a global climate change on Jupiter. *Nature,* **428,** 828–831.

Masuda, A., and K. Miki, 1995: On the stability of baroclinic vortex streets composed of quasi-geostrophic point eddies. *Deep-Sea Res. I,* **42,** 437–453.

Moore, D., and P. Saffman, 1971: Structure of a line vortex in an imposed strain. *Aircraft Wake Turbulence and its Detection,* J. H. Olsen, A. Goldburg, and H. Rogers, Eds., Plenum Press, 339–354.

Morales-Juberias, R., A. Sanchez-Lavega, J. Lecacheux, and F. Colas, 2002: A comparative study of Jovian cyclonic features from a six-year (1994–2000) survey. *Icarus,* **160,** 325–335.

——, ——, and T. E. Dowling, 2003: EPIC simulations of the merger of Jupiter's White ovals BE and FA: Altitude-dependent behavior. *Icarus,* **166,** 63–74.

Panetta, R. L., 1993: Zonal jets in wide baroclinically unstable regions: Persistence and scale selection. *J. Atmos. Sci.,* **50,** 2073–2106.

Polvani, L. M., J. Wisdom, E. deJong, and A. P. Ingersoll, 1990: Simple dynamical models of Neptune's Great Dark Spot. *Science,* **249,** 1393–1398.

Pouquet, A., M. Lesieur, J. C. Andre, and C. Basdevant, 1975: Evolution of high Reynolds number two-dimensional turbulence. *J. Fluid Mech.,* **75,** 305–319.

Pullin, D. I., 1998: Vortex dynamics in turbulence. *Annu. Rev. Fluid Mech.,* **30,** 31–51.

Read, P. L., P. J. Gierasch, B. J. Conrath, A. Simon-Miller, T. Fouchet, and Y. H. Yamazaki, 2006: Mapping potential-vorticity dynamics on Jupiter. I: Zonal-mean circulation from Cassini and Voyager 1 data. *Quart. J. Roy. Meteor. Soc.,* **132,** 1577–1603.

Rogers, J. H., 1995: *The Giant Planet Jupiter.* Cambridge University Press, 418 pp.

——, and D. Herbert, 1991: The three White Ovals and adjacent belts in the South Temperate region of Jupiter, 1940–1990. *J. Br. Astron. Assoc.,* **101,** 351–360.

Saffman, P. G., 1992: *Vortex Dynamics.* Cambridge University Press, 328 pp.

Simon, A. A., and R. F. Beebe, 1996: Jovian tropospheric features—Wind field, morphology, and motion of long-lived systems. *Icarus,* **121,** 319–330.

Sommeria, J., S. D. Meyers, and H. L. Swinney, 1989: Laboratory model of a planetary eastward jet. *Nature,* **337,** 58–61.

Vallis, G. K., and M. E. Maltrud, 1993: Generation of mean flows and jets on a beta-plane and over topography. *J. Phys. Oceanogr.,* **23,** 1346–1362.

Van Buskirk, R., 1991: Quasigeostrophic vortices in zonal shear. Ph.D. thesis, Harvard University, 129 pp.

——, and P. S. Marcus, 1994: Spectrally accurate contour dynamics. *J. Comput. Phys.,* **115,** 302–318.

Williams, G., and T. Yamagata, 1984: Geostrophic regimes, intermediate solitary vortices and Jovian eddies. *J. Atmos. Sci.,* **41,** 453–478.

Youssef, A., and P. S. Marcus, 2003: The dynamics of Jovian white ovals from formation to merger. *Icarus,* **162,** 74–93.